Bidirectional thermotaxis in *Caenorhabditis elegans* is mediated by distinct sensorimotor strategies driven by the AFD thermosensory neurons

Linjiao Luo[a,b,1,2], Nathan Cook[c,3], Vivek Venkatachalam[b,3], Luis A. Martinez-Velazquez[c,3], Xiaodong Zhang[d,3], Ana C. Calvo[c], Josh Hawk[c], Bronwyn L. MacInnis[e], Michelle Frank[b], Jia Hong Ray Ng[b], Mason Klein[b], Marc Gershow[b], Marc Hammarlund[c], Miriam B. Goodman[e,1,2], Daniel A. Colón-Ramos[c,1,2], Yun Zhang[d,1,2], and Aravinthan D. T. Samuel[b,1,2]

[a]Key Laboratory of Modern Acoustics, Ministry of Education, Department of Physics, Nanjing University, Nanjing 210093, China; [b]Department of Physics and Center for Brain Science, Harvard University, Cambridge, MA 02138; [c]Program in Cellular Neuroscience, Neurodegeneration, and Repair, Department of Cell Biology, Yale University School of Medicine, New Haven, CT 06536; [d]Department of Organismic and Evolutionary Biology and Center for Brain Science, Harvard University, Cambridge, MA 02138; and [e]Department of Molecular and Cellular Physiology, Stanford University School of Medicine, Stanford, CA 94305

Edited* by Paul W. Sternberg, California Institute of Technology, Pasadena, CA, and approved January 8, 2014 (received for review August 13, 2013)

The nematode *Caenorhabditis elegans* navigates toward a preferred temperature setpoint (T_s) determined by long-term temperature exposure. During thermotaxis, the worm migrates down temperature gradients at temperatures above T_s (negative thermotaxis) and performs isothermal tracking near T_s. Under some conditions, the worm migrates up temperature gradients below T_s (positive thermotaxis). Here, we analyze positive and negative thermotaxis toward T_s to study the role of specific neurons that have been proposed to be involved in thermotaxis using genetic ablation, behavioral tracking, and calcium imaging. We find differences in the strategies for positive and negative thermotaxis. Negative thermotaxis is achieved through biasing the frequency of reorientation maneuvers (turns and reversal turns) and biasing the direction of reorientation maneuvers toward colder temperatures. Positive thermotaxis, in contrast, biases only the direction of reorientation maneuvers toward warmer temperatures. We find that the AFD thermosensory neuron drives both positive and negative thermotaxis. The AIY interneuron, which is postsynaptic to AFD, may mediate the switch from negative to positive thermotaxis below T_s. We propose that multiple thermotactic behaviors, each defined by a distinct set of sensorimotor transformations, emanate from the AFD thermosensory neurons. AFD learns and stores the memory of preferred temperatures, detects temperature gradients, and drives the appropriate thermotactic behavior in each temperature regime by the flexible use of downstream circuits.

Navigational behaviors provide a framework for exploring the interplay among sensorimotor circuits, learning, and memory. During a navigational task, animals eventually reach their goals by implementing strategies composed of sensorimotor rules. Experience can modify navigational goals, so memory can also be integrated into sensorimotor pathways. Studying navigation in the nematode *Caenorhabditis elegans* offers the possibility of understanding the plasticity and programming of sensorimotor circuits from input to output in a small nervous system (1).

Previous studies established *C. elegans* thermotaxis as a model for experience-dependent navigation (2–6). When worms are exposed to specific temperatures between 15 °C and 25 °C for at least 4 h, they adopt those temperatures as their thermotactic setpoint (T_s) (2, 3, 5, 7). When placed on a spatial temperature gradient, worms seek the T_s. When arriving near T_s, worms track isotherms. Genetic analysis of thermotaxis has yielded mutants that are athermotactic (crawling randomly on temperature gradients), cryophilic (crawling to the coldest point on a temperature gradient irrespective of T_s), or thermophilic (crawling to the warmest point on a temperature gradient). This observation led to the suggestion that thermotaxis might involve separate circuits for negative thermotaxis (movement down gradients) and positive thermotaxis (movement up gradients) that balance near T_s (2, 4).

Systematic laser ablation analysis uncovered an interconnected neural circuit for thermotaxis behavior composed of one pair of thermosensory neurons (AFD) and three pairs of interneurons (AIY, AIZ, and RIA) (Fig. 1*A*) (4). Ablation of AFD or AIY led to cryophilic behavior. Ablation of AIZ led to thermophilic behavior. Ablation of RIA led to athermotactic behavior. Ablation of the AWC olfactory neuron, which is presynaptic to AIY and RIA, has also been found to mildly disrupt negative thermotaxis (8). These findings suggested that candidate circuit pathways converging on RIA might drive positive and negative thermotaxis (Fig. 1*A*).

Recently, movie microscopy has enabled high-resolution and high-content tracking of worm navigation (5, 9–12). Tracking negative thermotaxis and isothermal tracking have uncovered

Significance

The nematode *Caenorhabditis elegans* offers the opportunity to map complex behaviors to the specific roles of each neuron in a 302-neuron nervous system. Thermotaxis is a complex behavior where the worm inverts the behavioral mode—positive thermotaxis up gradients or negative thermotaxis down gradients—to move toward a remembered temperature. How are both long-term memory and multiple behavioral modes encoded? A long-standing model has been that separate circuits for positive and negative thermotaxis compete for control of body movement. In contrast, we find that different modes of thermotaxis are driven by one set of AFD thermosensory neurons. Circuits for different thermotactic behaviors diverge from the AFD neurons, probably by coupling sensory inputs to motor programs in different ways to create different thermotactic behaviors.

Author contributions: L.L., V.V., M.B.G., D.A.C.-R., Y.Z., and A.D.T.S. designed research; L.L., N.C., V.V., L.A.M.-V., A.C.C., J.H., B.L.M., M.F., and J.H.R.N. performed research; L.L., V.V., X.Z., A.C.C., J.H., B.L.M., M.K., M.G., and M.H. contributed new reagents/analytic tools; L.L. and V.V. analyzed data; and L.L., M.B.G., D.A.C.-R., Y.Z., and A.D.T.S. wrote the paper.

The authors declare no conflict of interest.

*This Direct Submission article had a prearranged editor.

[1]L.L., M.B.G., D.A.C.-R., Y.Z., and A.D.T.S. contributed equally to this work.

[2]To whom correspondence may be addressed. E-mail: samuel@physics.harvard.edu, lluo@fas.harvard.edu, mbgoodman@stanford.edu, daniel.colon-ramos@yale.edu, or yzhang@oeb.harvard.edu.

[3]N.C., V.V., L.A.M.-V., and X.Z. contributed equally to this work.

This article contains supporting information online at www.pnas.org/lookup/suppl/doi:10.1073/pnas.1315205111/-/DCSupplemental.

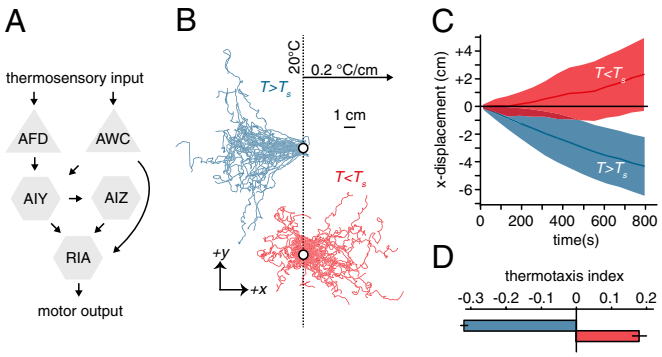

Fig. 1. Bidirectional thermotaxis in *C. elegans*. (*A*) A proposed neural circuit for thermotaxis showing chemical synaptic connectivity between the AFD and AWC sensory neurons and downstream interneurons. (*B*) Navigation trajectories over 15 min of 50 wild-type (N2) worms grown at 15 °C (blue) or 25 °C (red) and started near 20 °C on a 0.2 °C/cm linear spatial temperature gradient on a 22- × 22-cm agar plate (Fig. S1). Trajectories are aligned to the same starting point (white circle) for presentation purposes. (*C*) Mean *x* displacement ± 1 SD for trajectories shown in *B*. (*D*) A navigational index was computed for each trajectory using the component of velocity in the direction of the gradient divided by the mean crawling speed along each trajectory. Positive and negative thermotaxis corresponds to positive and negative indices, respectively. The magnitude of the index for negative thermotaxis is significantly larger than that for positive thermotaxis ($P < 0.0005$ using Student *t* test). All data points in *C* and *D* represent mean ± 1 SEM. Each calculation is based on at least 241 worm trajectories.

components of the worms' underlying behavioral strategies (12–14). Negative thermotaxis involves modulation of run length that is reminiscent of the biased random walk that was originally observed in bacterial chemotaxis (15, 16). In isotropic environments, worms move in a sequence of forward movements (runs) interrupted by turns and reversal turns (also called pirouettes) generating exploration that resembles an unbiased random walk. During negative thermotaxis, if worms sense negative temperature gradients, they suppress turns and reversal turns, yielding long runs in the favorable cooler direction. If worms sense positive temperature gradients, they exhibit short runs. Thus, net migration is down temperature gradients (13). Isothermal tracking is deterministic, a steering behavior in which the worm continuously makes temperature comparisons and movement corrections with every undulation to maintain isothermal alignment (14).

The strategy for positive thermotaxis has not yet been analyzed because this behavior is restricted to certain growth and stimulus conditions. If worms are grown at ~23 °C or higher, they will crawl up temperature gradients toward their T_s as long as they are within ~5 °C and navigating gradients are shallower than 0.5 °C/cm. Lower setpoints, steeper gradients, and greater distances from the T_s lead to athermotactic behavior (17). Now that we know specific conditions that evoke positive thermotaxis, we can use these conditions to compare and contrast the strategies for positive and negative thermotaxis.

Genetic methods provide tools to inactivate or remove specific neurons from *C. elegans* that yield larger numbers of animals than is possible with laser ablation. Cell-specific expression of reconstituted caspase (recCaspase) induces programmed cell death and thus the removal of specific neurons during development (18). Expression and irradiation of the protein KillerRed with intense green light remove cells acutely (19, 20). Here, we combine these methods with quantitative behavioral tracking to assess how each neuron in the proposed circuit for thermotaxis (AFD-AWC-AIY-AIZ-RIA) contributes to movement up or down temperature gradients.

We find that positive thermotaxis involves biased reorientation toward the T_s: the worm uses turns and reversal turns to point itself toward warmer temperatures. We find that negative thermotaxis also involves biased reorientation toward the T_s: the worm uses turns and reversal turns to point itself toward colder temperatures. As observed earlier, negative thermotaxis also involves a biased random walk toward the T_s, with longer runs toward colder temperatures and shorter runs toward warmer temperatures. These results suggest an asymmetry in the sensorimotor strategies for positive and negative thermotaxis, where run-length modulation makes negative thermotaxis more efficient by prolonging favorable orientations. We find that AFD drives both positive and negative thermotaxis. AIY is necessary to exhibit positive instead of negative thermotaxis below T_s. Although AWC, AIZ, and RIA might have minor contributions to thermotaxis, none of these neurons is required for either positive or negative thermotaxis. In summary, bidirectional thermotaxis emanates from the AFD neurons, achieved by coupling sensory input to motor output in different patterns to drive thermotaxis up gradients below T_s and down gradients above T_s.

Results

Strategies for Negative and Positive Thermotaxis Behaviors. We used high-pixel density movie cameras to record the movements of individual young adult worms performing thermotaxis across the surfaces of 22- × 22-cm agar plates with a shallow linear spatial temperature gradient (0.2 °C/cm) centered near 20 °C. With this gradient steepness and starting temperature, worms grown at 25 °C will move toward the warm side of the plate and worms grown at 15 °C will move toward the cold side of the plate, pursuing T_s in either direction (Fig. 1 *B* and *C*) (17). Large space for thermotaxis allowed us to study many worms at once. High-pixel density cameras allowed us to segment trajectories based on worm posture, even at low magnification, into a sequence of periods of forward movement, backward movement, and sharp turns. In this setup, many uninterrupted thermotaxis trajectories of individual worms can be obtained in each experiment, increasing the quality of statistical analysis.

An index of thermotaxis efficiency is provided by the ratio between the mean velocity in the gradient direction of each trajectory and crawling speed: $\langle v_x \rangle / \langle s \rangle$ (Fig. 1*D*). This index is +1 if the worm strictly moves straight up the gradient and −1 if it strictly moves straight down the gradient. We found that negative thermotaxis is more efficient than positive thermotaxis. To better understand this, we turned to detailed analysis of individual animal movements. Net movement up or down gradients is the product of sensorimotor rules enacted along the navigational trajectory. We sought to extract these rules for positive and negative thermotaxis.

In isotropic environments, crawling locomotion is an alternating sequence of periods of forward movement (runs) and reorientation maneuvers. Reorientation maneuvers are either turns or reversal turns (also called pirouettes) (12, 13, 15) (Fig. 2 *A* and *B* and Movie S1). First, we examined the statistics of run duration, the time intervals between successive reorientation maneuvers. As before for negative thermotaxis, we found that worms exhibited longer runs when headed down gradients than up gradients (11–13, 21) (Fig. 2*C*). During positive thermotaxis, run durations were roughly the same whether up or down gradients (Fig. 2*C*).

Next, we examined the possibility of steering to select favorable directions either during runs or by reorientation maneuvers. Steering mechanisms (also called weathervaning) have been identified in *C. elegans* chemotaxis (11, 21, 22). To look for steering mechanisms, we focused on runs pointed orthogonally to the gradient. If the worm was capable of steering during a run, the run should gradually veer toward preferred directions. However, we found that runs veered toward the preferred and nonpreferred directions by similar amounts during either negative or positive thermotaxis (Fig. 2*D*). If the worm used reorientation maneuvers to pick the direction of new runs after runs pointed orthogonally to the gradient, it should be able to bias new runs to be up the gradient during positive thermotaxis or down the gradient during negative thermotaxis. For both positive

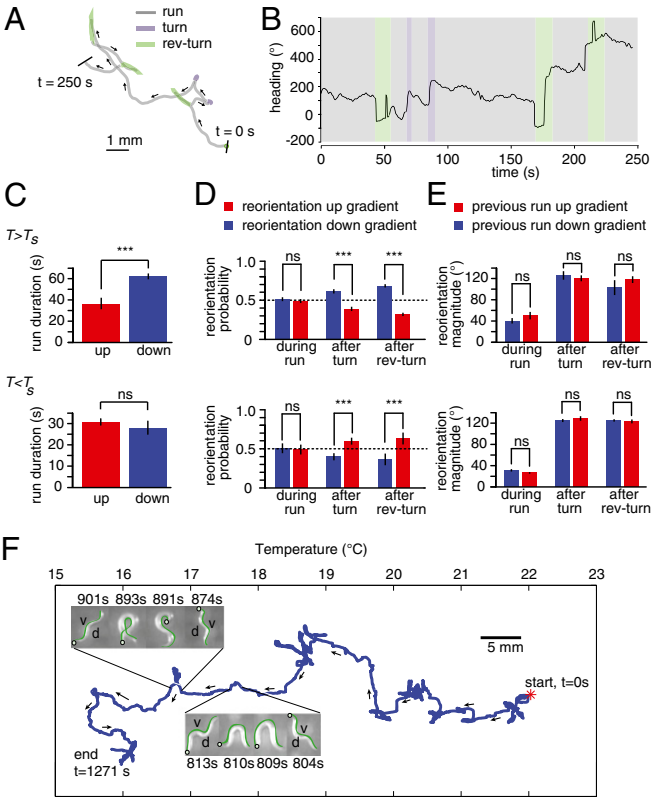

Fig. 2. Strategies for bidirectional thermotaxis. (*A*) Representative 250-s trajectory of a crawling worm segmented using machine-vision software that detects forward movements (gray), turns (purple), and reversal turns (green) on the basis of posture and movement (*Materials and Methods* and Movie S1). (*B*) Orientation with respect to the gradient is continuously monitored for each worm during thermotaxis (data for trajectory in *A* is represented), and the frequency, direction, and size of reorientation maneuvers are calculated to assess navigational strategy. For presentation purposes, the orientation angle is unwrapped so that continuous changes in heading that pass through 0° do not cause 360° jumps. (*C*) During negative thermotaxis (*Upper*), runs down the temperature gradient (blue) are longer than runs up the gradient (red). During positive thermotaxis (*Lower*), runs up and down the gradient are in the same duration. Calculations are based on runs with orientations within 45° of the gradient axis. (*D*) During negative thermotaxis (*Upper*) or positive thermotaxis (*Lower*), runs orthogonal to the gradient veer toward warmer temperatures and colder temperatures with equal likelihood. After runs orthogonal to the gradient, the worm uses reorientation maneuvers to bias new runs toward preferred temperatures. (*E*) During negative (*Upper*) or positive thermotaxis (*Lower*), the size of angular reorientation between the beginning and end of runs down the gradient are the same as for runs up the gradient. The size of angular reorientation after turns or reversal turns that terminate runs down the gradient are the same size as those for runs up the gradient. All data points in *C*–*E* represent mean ± 1 SEM. Calculations are based on runs with orientations within 45° of the gradient axis taken from 241 to 309 worm trajectories. ***$P < 0.0005$ using Student *t* test. ns, no significant difference. (*F*) A representative center-of-mass trajectory of an individual wild-type young adult worm grown at 15 °C and started at 22 °C on a linear temperature gradient is shown. Movements on a spatial gradient were tracked on a compound microscope (*Materials and Methods*). During negative thermotaxis, the animal uses turns and reversal turns to orient itself toward colder temperatures. For this animal viewed from above, reorientation maneuvers that produced clockwise or counterclockwise heading changes involved ventral or dorsal bending, respectively. Portions of the trajectory are highlighted that involve a turn with dorsal bending (804–813 s) and a reversal turn with ventral bending (874–901 s). In each frame, the head is labeled with a circle and the ventral side is labeled with a green line. Similar trajectories were observed in a total of 10 individual worms.

and negative thermotaxis, we found that both turns and reversal turns were more likely to point new runs toward the T_s (Fig. 2*D*).

We also examined the size of heading changes, both by gradual reorientation during runs and by reorientation maneuvers. A plausible navigation mechanism is to make small heading changes when already headed in favorable directions, but larger heading changes when headed in unfavorable directions. This strategy is exhibited by *Drosophila* larva during thermotaxis (4, 22). However, we found no evidence that the size of heading changes was affected by initial orientation during thermotaxis (Fig. 2*E*).

Crawling worms lie on their left or right side, and thus steering to orient the animal toward preferred temperatures must involve bending toward the dorsal or ventral side. A high-resolution analysis of salt chemotaxis—carried out by monitoring the bending movements of worms subjected to chemical currents while held in microfluidic devices—has shown that worms can bend both dorsally and ventrally toward attractants (23). The large-format assay that we used to quantify thermotactic strategies (Fig. 2) lacks resolution to label the dorsal and ventral sides of each crawling animal. To look more closely at steering, we made a single-animal tracking system by placing a spatial temperature gradient on the motorized stage of a compound microscope. We found that reorientation maneuvers using both dorsal and ventral bending movements appeared along thermotactic trajectories (Fig. 2*F*).

Taken together, our results suggest that negative thermotaxis involves two strategies. During negative thermotaxis, the worm extends runs toward colder temperatures and shortens runs toward warmer temperatures and uses reorientation maneuvers to increase the likelihood that new runs are pointed toward colder temperatures. During positive thermotaxis in our setup, the worm relies on reorientation maneuvers to point runs toward warmer temperatures.

AFD Thermosensory Neuron Drives Both Positive and Negative Thermotaxis. The principal thermosensory neurons in *C. elegans* are the AFD neurons, a bilateral pair that send sensory dendrites toward the amphid pore near the anterior tip of the worm. AFD was discovered to be involved in thermotaxis through laser ablation analysis. Killing AFD caused worms to either move to the coldest part of a temperature gradient (a cryophilic phenotype) or not to exhibit a thermal preference at all (an athermotactic phenotype). Killing AFD also abolished isothermal tracking behavior (4, 24).

A more recent laser ablation analysis of AFD quantified turn frequency, a measure of the biased random walk during negative thermotaxis. Swimming worms were exposed to warming or cooling temporal ramps at temperatures above or below the T_s (12, 24). Killing AFD disrupted the temperature-dependent modulation of turn frequency when worms should exhibit negative thermotaxis above T_s. Killing AFD did not create any turn frequency bias at temperatures below the T_s. The analysis of turn frequency in swimming worms subjected to temporal ramps would be sensitive only to the modulation of run duration, and the absence of a biased random walk component in positive thermotaxis (see above) may explain why the swimming assay has revealed only negative thermotaxis (12, 24). Because our experimental conditions allow us to examine and compare both positive and negative thermotaxis, we investigated the role of AFD in driving thermotaxis both above and below the T_s.

First, we used a genetic method to remove AFD by selectively expressing recCaspase (18). Coexpression of two subunits of the *C. elegans* CED-3 Caspase under the control of the AFD-specific promoter *gcy-8* leads to AFD cell death. We found that killing AFD diminished both positive and negative thermotaxis, suggesting that AFD regulates both behaviors (Fig. 3*A*). We also used an independent method of cell ablation with KillerRed, a photosensitive protein that kills cells upon green light illumination (25). We used transgenic lines that selectively expressed KillerRed in the AFD neurons and compared irradiated and nonirradiated animals 1 d after exposure. We verified destruction of the AFD neurons in the irradiated animals using

fluorescence microscopy. Consistent with recCaspase-mediated AFD ablation, we found that movements up and down thermal gradients were disrupted by KillerRed-mediated AFD ablation (Fig. 3*A*). We also examined a mutant, *ttx-1(p767)*, with a developmental defect in AFD owing to a mutation in the Otx/otd homolog *ttx-1* gene. Previously, it was shown that mutations in *ttx-1* diminished negative thermotaxis above the T_s and produced weak negative thermotaxis below the T_s (26). In our experimental setup, we found that *ttx-1*–mediated disruption of AFD development weakened negative thermotaxis above T_s and abolished positive thermotaxis below T_s (Fig. 3*A*). We note that the *ttx-1 (p767)* allele disrupts AFD development without completely removing the neuron (26), which may explain the difference caused by partial loss of thermotactic movement by *ttx-1* mutation and complete loss by ablation.

Analysis of Other Neurons in the Proposed Neural Circuit for Thermotaxis. In the classic model for the thermotaxis neural circuit, competing circuits for positive and negative thermotaxis are integrated by downstream interneurons (4, 27). In particular, AIY and AIZ were proposed to drive positive and negative thermotaxis, respectively; RIA was proposed to integrate both pathways (Fig. 1*A*) (28). Next, we examined the contributions of these interneurons to positive and negative thermotaxis using our experimental setup.

We examined AIY using three different methods of cell disruption, the *ttx-3(ks5)* mutant that disrupts AIY development, and transgenic lines that specifically expressed recCaspase or KillerRed to remove AIY. In all three cases, we found that these worms moved down temperature gradients instead of moving up gradients when started at temperatures below the T_s (Fig. 3*B*). Laser ablation of AIZ has been reported to cause a thermophilic phenotype: worms lacking AIZ crawled to the warmest point on a spatial temperature gradient (4). Cell-specific promoters are not available for AIZ, and so we used laser ablation to remove it. We found no evidence that AIZ removal generated thermophilic movement (Fig. 3*B*). Laser ablation of RIA has been reported to abolish thermotaxis at all temperatures (4). We used two strategies for RIA ablation: cell-specific expression of recCaspase and of KillerRed. We found that destroying RIA in developed worms using KillerRed had no effect on thermophilic or cryophilic movement. Killing RIA with recCaspase had no effect on positive thermotaxis, but may reduce negative thermotaxis above the T_s. In any case, RIA is not required for worms to exhibit positive or negative thermotaxis in our experimental setup (Fig. 3*B*).

Ablation of the AWC olfactory neurons has been reported to mildly disrupt negative thermotaxis down gradients toward the T_s (8). Because our setup supports both positive and negative thermotaxis, we examined AWC using both laser ablation and cell-specific expression of recCaspase. We found no significant disruption in either positive or negative thermotaxis after AWC removal (Fig. 3*B*).

AFD Drives Thermotactic Behavior in Both Thermophilic and Cryophilic Animals. Our results indicate that AFD regulates both positive and negative thermotaxis toward the T_s. We asked whether AFD also drives these behaviors in worms that aberrantly display positive thermotaxis by moving toward warmer temperatures even when above T_s (i.e., a thermophilic phenotype) or negative thermotaxis by moving toward colder temperatures even when below T_s (i.e., a cryophilic phenotype).

We performed a forward genetic screen to identify mutants that exhibited a strong thermophilic phenotype and isolated *pg5*, which robustly migrated up steep thermal gradients following cultivation at 15 °C and 25 °C (Fig. 3*C*). Three-factor and snip-SNP mapping placed the *pg5* mutation on the right side of chromosome V near the position of *pkc-1*. *pkc-1* (also known as *ttx-4*) has previously been implicated in thermotaxis (7). Complementation with a putative null allele, *nj1*, revealed that *pg5* was an allele of *pkc-1*, as *pg5/nj1* heterozygotes exhibited behavior that was indistinguishable from that of either mutant alone. Sequencing the *pkc-1* gene in *pg5* worms revealed a single nucleic acid substitution in the fifth exon, introducing a premature stop codon and indicating that *pg5* is likely to be a null allele of *pkc-1*. No other thermophilic mutants were isolated in the screen.

It has been shown that AFD-specific expression of wild-type *pkc-1* rescues its thermotaxis defect, suggesting that PKC signaling in AFD contributes to the display of negative vs. positive thermotaxis (7). To determine whether AFD output is needed to drive thermophilic movement in *pkc-1* mutants, we used a transgenic line that expressed recCaspase in AFD in a *pkc-1(pg5)* mutant background. Indeed, AFD ablation abolished thermotaxis both above and below the T_s (Fig. 3*C*).

Next, we asked whether AFD was required to produce negative thermotaxis in worms lacking the AIY interneuron, resulting either from mutation in *ttx-3(ks5)* or from genetic ablation of

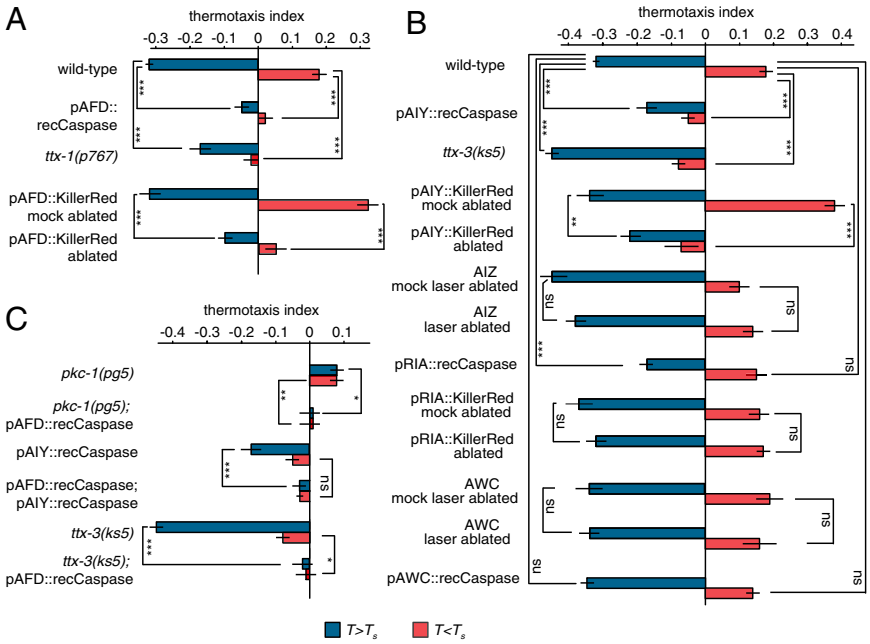

Fig. 3. Neuronal determinants of thermotaxis. (*A*) Analysis of AFD contributions to negative thermotaxis when $T > T_s$ and to positive thermotaxis when $T < T_s$. (*B*) Analysis of other neurons in the proposed circuit for thermotaxis. (*C*) Analysis of AFD in mutant backgrounds that always crawl up or down temperature gradients. The thermotactic index—the ratio between mean velocity in the gradient direction and mean crawling speed (mean ± 1 SEM)—is calculated over the trajectories of individual worms when started at 20 °C and grown at 25 °C (red, $T < T_s$) or when started at 20 °C and grown at 15 °C ($T > T_s$). Salient comparisons between worms with intact neurons or disrupted neurons are shown. $^*P < 0.05$; $^{**}P < 0.005$; $^{***}P < 0.0005$ by Student *t* test. A total of 40–309 worms were used to calculate each index.

AIY. We found that AFD-specific expression of recCaspase in either a *ttx-3(ks5)* background or a AIY::recCaspase background disrupted negative thermotaxis at all temperatures (Fig. 3*C*).

In summary, AFD is needed to drive movement above and below T_s in both mutant and wild-type animals. Disrupting PKC signaling causes positive thermotaxis to emanate from AFD above T_s, whereas loss of the AIY interneuron causes negative thermotaxis to emanate from AFD below T_s via other circuit pathways.

AFD Responds to Temperatures That Span Both Negative and Positive Thermotaxis. Calcium imaging of the AFD neuron in response to temperature waveforms has shown that the operating range of AFD spans the range of isothermal tracking and cryophilic behavior. At temperatures near and above the T_s, warming will depolarize AFD and cause an increase in intracellular calcium level whereas cooling will hyperpolarize AFD and cause a decrease in the calcium levels (29–32).

For AFD to drive bidirectional movement on thermal gradients, it has to be active at temperatures several degrees below 25 °C for worms grown at 25 °C and above 15 °C for worms grown at 15 °C. To test this, we used transgenic worms that express the calcium-sensitive protein G-CaMP6s (33) in the AFD neurons in wild-type animals, two constitutively cryophilic strains [a transgenic line that expresses recCaspase in AIY and the *ttx-3 (ks5)* mutant], and a thermophilic strain [*pkc-1(pg5)*]. When worms are exposed to a linearly increasing temperature with a superimposed sinusoidal oscillation, AFD will phase-lock to the sinusoidal component at temperatures near and above the T_s. The lower bound of AFD calcium dynamics can be changed by cultivating worms at different temperatures (3, 31). We found that, when wild-type or mutant worms were grown at 15 °C, AFD calcium dynamics extended from 15 °C to higher temperatures, overlapping the normal range of negative thermotaxis (Fig. 4 *A* and *B*). When worms were grown at 25 °C, AFD calcium dynamics extended from ∼21 °C to higher temperatures, overlapping the normal range of positive thermotaxis. Thus, AFD activity spans the range of both positive and negative thermotaxis exhibited by wild-type worms. Neither the mutation *pkc-1(pg5)* nor *ttx-3(ks5)* that caused thermophilic and cryophilic behavior affect temperature-evoked AFD calcium dynamics, suggesting that the effects of these mutations in regulating switching between negative and positive thermotaxis are farther downstream (Fig. 4*B*).

Discussion

C. elegans thermotaxis is a complex behavior where different modes of navigation are carried out under different temperature regimes, suggesting that experience-dependent mechanisms allow sensory inputs to be transformed into motor outputs in different patterns depending on context. Here, we examine the two opposite modes of thermotaxis, negative and positive thermotaxis, under experimental conditions that support movement either down or up temperature gradients toward the preferred temperature. We find that different sensorimotor transformations are used for each behavior. During negative thermotaxis, the worm modulates the rate of reorientation maneuvers (turns and reversal turns) to lengthen runs toward cooler temperatures; additionally, the worm uses its reorientation maneuvers to point new runs toward cooler temperatures. During positive thermotaxis, the worm relies on reorientation maneuvers to point new runs toward warmer temperatures.

The AFD neuron is required for both negative and positive thermotaxis. Interestingly, temperature-evoked calcium dynamics in AFD span the range of both positive and negative thermotaxis exhibited by wild-type worms; AFD calcium levels are raised by warming and lowered by cooling in essentially the same way across its activity range. We also found that AFD calcium dynamics are unaffected by several mutations that induce strong cryophilic or thermophilic phenotypes (Fig. 4 *A* and *B*). Collectively, these results suggest that circuit pathways linking sensation to positive and negative thermotaxis diverge downstream of

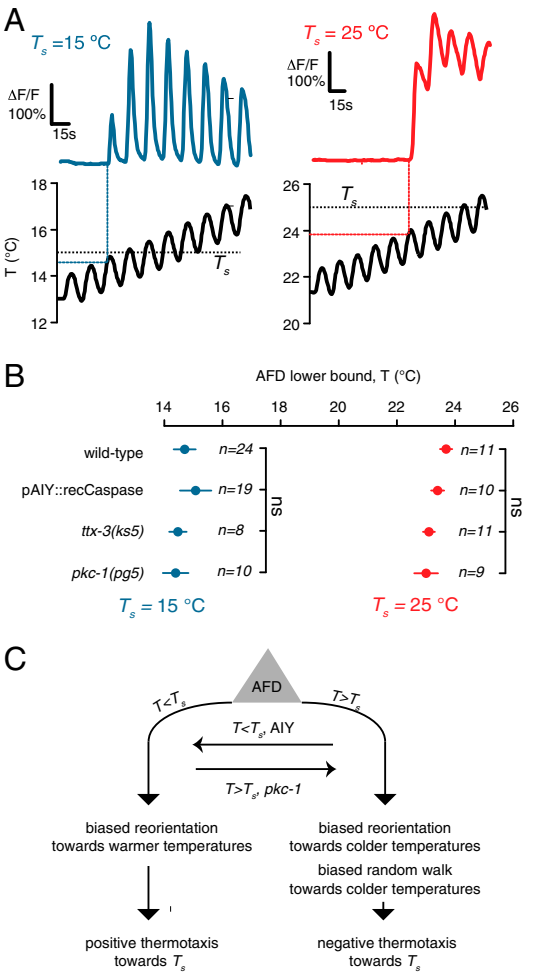

Fig. 4. AFD is activated above the setpoint for worms grown at 15 °C and below the setpoint for worms grown at 25 °C. (*A*) Immobilized worms expressing GCaMP6s in the AFD neurons grown at 15 °C (*Left*) or 25 °C (*Right*) are subjected to linearly increasing temperatures with a superimposed sinusoidal variation. AFD calcium dynamics begin to phase-lock to the sinusoidal component at specific temperatures above the T_s when worms are grown at 15 °C (overlapping the range of negative thermotaxis) and below the T_s when worms are grown at 25 °C (overlapping the range of positive thermotaxis). (*B*) The onset temperature of AFD calcium dynamics for worms exposed to temperature variations as shown in *A* is indistinguishable in mutants lacking AIY interneurons owing to cell-specific expression of recCaspase, the cryophilic mutant *ttx-3*, or the thermophilic mutant *pkc-1 (pg5)*. The numbers of worms used for each experiment are shown next to each data point. Data points represent mean onset temperature ±1 SEM. "ns" indicates no statistical difference between each mutant and wild type. (*C*) Bidirectional thermotaxis emanates from the AFD neuron. Positive thermotaxis emanates from AFD $T < T_s$. Negative thermotaxis emanates from AFD when $T > T_s$. AIY may help switch AFD output from driving negative thermotaxis to positive thermotaxis when $T < T_s$. The gene *pkc-1 (pg5)* may help switch AFD output from driving positive thermotaxis to negative thermotaxis when $T < T_s$. The sensorimotor transformations that generate each thermotaxis behavior are summarized.

AFD. For example, to shift behavior from negative to positive thermotaxis, downstream circuits might inactivate the mechanism that modulates run length and invert the mechanism for reorientation direction from a bias toward colder temperatures to a bias toward warmer temperatures (Fig. 4*C*).

The main postsynaptic output of AFD is the AIY interneuron (34). Simultaneous optogenetic stimulation of AFD and electrophysiological recording of AIY has revealed that synaptic output from AFD to AIY involves both glutamatergic and

peptidergic signals (35, 36). One possibility is that AIY acts as a switch, shifting AFD output from driving negative thermotaxis to positive thermotaxis below the setpoint. The function of *pkc-1* acting in AFD may also contribute to the switching mechanism, helping to shift AFD output from driving positive thermotaxis to negative thermotaxis above the setpoint (Fig. 4*C*). Although AIY is the dominant postsynaptic partner of AFD, it is not needed to carry out the sensorimotor transformations that transform AFD activity into negative thermotaxis. The AWC olfactory neuron and the AIZ interneuron have been proposed to play roles in negative thermotaxis (4, 8, 27); we find that neither AWC nor AIZ is required for either positive or negative thermotaxis. RIA has been proposed to be required for both positive and negative thermotaxis (4). RIA has recently been found to represent a corollary discharge signal that conveys head movement to the upstream circuit (37). We do not believe that RIA plays an essential role in the thermotaxis behavior probed in our assays.

In summary, different modes of thermotaxis are driven by the AFD thermosensory neurons via different sensorimotor strategies. AFD intracellular signaling is sophisticated, involving a complex cGMP-dependent thermotransduction cascade and multiple forms of synaptic output including glutamatergic signaling, peptidergic signaling, and gap junctions (35, 36, 38, 39). The richness of AFD signal processing and synaptic output is likely to underlie its capacity to effect the appropriate mode of thermotactic behavior in different temperature regimes via downstream circuits that flexibly map AFD activity patterns to movement patterns.

Materials and Methods

Strains, Cultivation, and Ablation Methods. *C. elegans* were grown on bacterial lawns of the *Escherichia coli* strain OP50 overnight at 15 °C or 25 °C using standard methods (40). Strains used and the procedure for isolating the allele *pkc-1(pg5)* are described in *SI Materials and Methods*. Laser ablation, KillerRed-mediated ablation, and Caspase-mediated ablation were performed using previously described methods, described in detail in *SI Materials and Methods* (18, 19, 41).

Behavioral Analysis. High-throughput behavioral analysis using a large-format thermotaxis assay was devised by adapting previously described methods used for analyzing the navigational movements of *C. elegans* or *Drosophila* larva (12, 42). The high-resolution behavioral assay was generated by using a smaller version of the high-throughput behavioral assay mounted on a compound microscope. Descriptions of the apparatus and software are available in *SI Materials and Methods*.

Calcium Imaging. Calcium imaging followed previously described protocols for measuring the activity of the AFD neurons (31). Custom hardware for temperature control and spinning disk confocal microscopy that was used in this study is described in *SI Materials and Methods*. Data analysis was performed using MATLAB (Mathworks).

ACKNOWLEDGMENTS. This work was supported by National Science Foundation (NSF) Grant PHY-0957185 and National Institutes of Health (NIH) Grant 8DP1GM105383-05 (to A.D.T.S.), NSF Grant IOS0725079 and NIH Grant R21 NS061147 (to M.B.G.), a Human Frontier Science Program fellowship (to B.L.M.), NIH Grant 1P01GM103770 (to A.D.T.S. and Y.Z.), National Nature Science Foundation of China Grant 11304153 (to L.L.), and NIH Grant R01NS076558 (to D.A.C.-R.).

1. de Bono M, Maricq AV (2005) Neuronal substrates of complex behaviors in C. elegans. *Annu Rev Neurosci* 28:451–501.
2. Hedgecock EM, Russell RL (1975) Normal and mutant thermotaxis in the nematode Caenorhabditis elegans. *Proc Natl Acad Sci USA* 72(10):4061–4065.
3. Biron D, et al. (2006) A diacylglycerol kinase modulates long-term thermotactic behavioral plasticity in C. elegans. *Nat Neurosci* 9(12):1499–1505.
4. Mori I, Ohshima Y (1995) Neural regulation of thermotaxis in Caenorhabditis elegans. *Nature* 376(6538):344–348.
5. Chi CA, et al. (2007) Temperature and food mediate long-term thermotactic behavioral plasticity by association-independent mechanisms in C. elegans. *J Exp Biol* 210(Pt 22):4043–4052.
6. Kimata T, Sasakura H, Ohnishi N, Nishio N, Mori I (2012) Thermotaxis of C. elegans as a model for temperature perception, neural information processing and neural plasticity. *Worm* 1(1):31–41.
7. Okochi Y, Kimura KD, Ohta A, Mori I (2005) Diverse regulation of sensory signaling by C. elegans nPKC-epsilon/eta TTX-4. *EMBO J* 24(12):2127–2137.
8. Biron D, Wasserman S, Thomas JH, Samuel ADT, Sengupta P (2008) An olfactory neuron responds stochastically to temperature and modulates Caenorhabditis elegans thermotactic behavior. *Proc Natl Acad Sci USA* 105(31):11002–11007.
9. Swierczek NA, Giles AC, Rankin CH, Kerr RA (2011) High-throughput behavioral analysis in C. elegans. *Nat Methods* 8(7):592–598.
10. Stephens GJ, Johnson-Kerner B, Bialek W, Ryu WS (2008) Dimensionality and dynamics in the behavior of C. elegans. *PLOS Comput Biol* 4(4):e1000028.
11. Albrecht DR, Bargmann CI (2011) High-content behavioral analysis of Caenorhabditis elegans in precise spatiotemporal chemical environments. *Nat Methods* 8(7):599–605.
12. Clark DA, Gabel CV, Lee TM, Samuel ADT (2007) Short-term adaptation and temporal processing in the cryophilic response of Caenorhabditis elegans. *J Neurophysiol* 97(3):1903–1910.
13. Ryu WS, Samuel ADT (2002) Thermotaxis in Caenorhabditis elegans analyzed by measuring responses to defined Thermal stimuli. *J Neurosci* 22(13):5727–5733.
14. Luo L, Clark DA, Biron D, Mahadevan L, Samuel ADT (2006) Sensorimotor control during isothermal tracking in Caenorhabditis elegans. *J Exp Biol* 209(Pt 23):4652–4662.
15. Pierce-Shimomura JT, Morse TM, Lockery SR (1999) The fundamental role of pirouettes in Caenorhabditis elegans chemotaxis. *J Neurosci* 19(21):9557–9569.
16. Berg HC, Brown DA (1972) Chemotaxis in Escherichia coli analysed by three-dimensional tracking. *Nature* 239(5374):500–504.
17. Ramot D, MacInnis BL, Lee H-C, Goodman MB (2008) Thermotaxis is a robust mechanism for thermoregulation in Caenorhabditis elegans nematodes. *J Neurosci* 28(47):12546–12557.
18. Chelur DS, Chalfie M (2007) Targeted cell killing by reconstituted caspases. *Proc Natl Acad Sci USA* 104(7):2283–2288.
19. Williams DC, et al. (2013) Rapid and permanent neuronal inactivation in vivo via subcellular generation of reactive oxygen with the use of KillerRed. *Cell Rep* 5(2):553–563.
20. Bulina ME, et al. (2006) A genetically encoded photosensitizer. *Nat Biotechnol* 24(1):95–99.
21. Iino Y, Yoshida K (2009) Parallel use of two behavioral mechanisms for chemotaxis in Caenorhabditis elegans. *J Neurosci* 29(17):5370–5380.
22. Luo L, et al. (2010) Navigational decision making in Drosophila thermotaxis. *J Neurosci* 30(12):4261–4272.
23. McCormick KE, Gaertner BE, Sottile M, Phillips PC, Lockery SR (2011) Microfluidic devices for analysis of spatial orientation behaviors in semi-restrained Caenorhabditis elegans. *PLoS ONE* 6(10):e25710.
24. Chung SH, Clark DA, Gabel CV, Mazur E, Samuel ADT (2006) The role of the AFD neuron in C. elegans thermotaxis analyzed using femtosecond laser ablation. *BMC Neurosci* 7:30.
25. Teh C, et al. (2010) Optogenetic in vivo cell manipulation in KillerRed-expressing zebrafish transgenics. *BMC Dev Biol* 10:110.
26. Satterlee JS, et al. (2001) Specification of thermosensory neuron fate in C. elegans requires ttx-1, a homolog of otd/Otx. *Neuron* 31(6):943–956.
27. Kuhara A, et al. (2008) Temperature sensing by an olfactory neuron in a circuit controlling behavior of C. elegans. *Science* 320(5877):803–807.
28. Mori I, Sasakura H, Kuhara A (2007) Worm thermotaxis: A model system for analyzing thermosensation and neural plasticity. *Curr Opin Neurobiol* 17(6):712–719.
29. Ramot D, MacInnis BL, Goodman MB (2008) Bidirectional temperature-sensing by a single thermosensory neuron in C. elegans. *Nat Neurosci* 11(8):908–915.
30. Kimura KD, Miyawaki A, Matsumoto K, Mori I (2004) The C. elegans thermosensory neuron AFD responds to warming. *Curr Biol* 14(14):1291–1295.
31. Clark DA, Biron D, Sengupta P, Samuel ADT (2006) The AFD sensory neurons encode multiple functions underlying thermotactic behavior in Caenorhabditis elegans. *J Neurosci* 26(28):7444–7451.
32. Clark DA, Gabel CV, Gabel H, Samuel ADT (2007) Temporal activity patterns in thermosensory neurons of freely moving Caenorhabditis elegans encode spatial thermal gradients. *J Neurosci* 27(23):6083–6090.
33. Chen T-W, et al. (2013) Ultrasensitive fluorescent proteins for imaging neuronal activity. *Nature* 499(7458):295–300.
34. White JG, Southgate E, Thomson JN, Brenner S (1986) The structure of the nervous system of the nematode Caenorhabditis elegans. *Philos Trans R Soc Lond B Biol Sci* 314(1165):1–340.
35. Ohnishi N, Kuhara A, Nakamura F, Okochi Y, Mori I (2011) Bidirectional regulation of thermotaxis by glutamate transmissions in Caenorhabditis elegans. *EMBO J* 30(7):1376–1388.
36. Narayan A, Laurent G, Sternberg PW (2011) Transfer characteristics of a thermosensory synapse in Caenorhabditis elegans. *Proc Natl Acad Sci USA* 108(23):9667–9672.
37. Hendricks M, Ha H, Maffey N, Zhang Y (2012) Compartmentalized calcium dynamics in a C. elegans interneuron encode head movement. *Nature* 487(7405):99–103.
38. Wang D, O'Halloran D, Goodman MB (2013) GCY-8, PDE-2, and NCS-1 are critical elements of the cGMP-dependent thermotransduction cascade in the AFD neurons responsible for C. elegans thermotaxis. *J Gen Physiol* 142(4):437–449.
39. Chuang C-F, Vanhoven MK, Fetter RD, Verselis VK, Bargmann CI (2007) An innexin-dependent cell network establishes left-right neuronal asymmetry in C. elegans. *Cell* 129(4):787–799.
40. Brenner S (1974) The genetics of Caenorhabditis elegans. *Genetics* 77(1):71–94.
41. Fang-Yen C, Gabel CV, Samuel ADT, Bargmann CI, Avery L (2012) Laser microsurgery in Caenorhabditis elegans. *Methods Cell Biol* 107:177–206.
42. Gershow M, et al. (2012) Controlling airborne cues to study small animal navigation. *Nat Methods* 9(3):290–296.

Supporting Information

Luo et al. 10.1073/pnas.1315205111

SI Materials and Methods

Strains. The wild-type strain (Bristol N2), *ttx-1(p767)*, and *ttx-3 (ks5)* mutant strains were obtained from the *Caenorhabditis* Genetics Center (University of Minnesota). Strains used to map and clone *pg5* are the following: *SP24 dpy-5(e61) unc-54(e190) I, MT588 lin-31(n301) unc-4(e120) II, SP17 unc-32(e189) dpy-1(e1) III, DR105 unc-17(e245) dpy-20(e1282) IV, DR181 unc-60(m35) dpy-11(e224) V, SP413 unc-7(e139) lon-2(e678) X, GN70 pgIR5 (V, N2 > CB4856) V*. Transgenic strains used in this study include the following: ZC1974 *yxEx1006[Pttx-3::MYRTDKrd; Punc-122::gfp]*, ZC1990 *yxEx1022[Pglr-3::MYRTDKrd; Punc-122::gfp]*, ZC2002 *yxEx1034[Pgcy-8::MYRTDKrd; Punc-122::gfp]*, TV3494 *wyEx1348[Pgcy-8::caspase-3(p12)::nz; Pgcy-8::cz::caspase-3(p17); Punc-122::gfp]*, TV6718 *wyIs111;wyEx1046[Pttx-3::cfp;Pgcy-8::rab-3::mCh;Pttx-3::caspase-3(p12)::nz;Pttx-3::cz::caspase-3(p17); Punc-122::rfp]*, DCR404 *olaEx212[Pgcy-8::caspase-3(p12)::nz;Pgcy-8::cz::caspase-3(p17);Pttx-3::caspase-3(p12)::nz;Pttx-3::cz::caspase-3(p17); Punc-122::gfp]*, DCR2589 *ttx-3(ot22);wyEx1348[Pgcy-8::caspase-3(p12)::nz;Pgcy-8::cz::caspase-3(p17);Punc-122::gfp]*, DCR2500 *pkc-1(pg5);wyIs45;wyEx1348[Pttx-3::rab-3::gfp;Punc-122::rfp;Pgcy-8::caspase-3(p12)::nz;Pgcy-8::cz::caspase-3(p17);Punc-122::gfp]*, TV2231 *wyEx828[Pglr-3::caspase-3(p12)::nz;Pglr-3::cz::caspase-3(p17);Pglr-3::mCherry;Punc-122::gfp]*, DCR1258 *olaEx743[Podr-2b(3a)::gfp]*, PY7502 *Pceh-36::caspase-3;Pstrx-1::gfp*, *otls264 Pceh-36::RFP*.

Mutant Screen. Wild-type, L4 hermaphrodite larvae were exposed to ethyl methanesulfonate (50 mM) for 3 h at room temperature. Young adult nonclonal F2 progeny were grown at 20 °C in the presence of abundant food and tested on a linear (1 °C/cm) thermal gradient (1) at a starting temperature of 23 °C. Worms that migrated to the warmest region of the assay plate within 10 min were picked to individual growth plates, and their progeny were tested for thermotaxis defects.

Mapping *pkc-1(pg5)*. *pg5* mutants were backcrossed six times to N2 before mapping. *pg5*/+ heterozygotes showed no defect in thermotaxis, indicating that the mutation is completely recessive. *pg5* was mapped to chromosome V using traditional three-factor mapping with visible (Dpy, Unc) markers. Subsequent snip-SNP mapping placed the *pg5* locus on the right arm of chromosome V. snip-SNP mapping for *pg5* was performed using a chromosome V substitution strain, GN70 *pgIR5* (V, CB4856 > N2), in which chromosome V from N2 was substituted by chromosome V from the standard reference strain for SNP mapping, CB4856 (2).

Ablation Methods. A MicroPoint high-intensity pulsed dye laser system (Andor Technology) was focused onto targeted neurons, and a controlled series of 440-nm pulses was delivered to destroy the neuron. Ablated and mock-ablated worms were recovered and cultivated overnight for testing the following day.

KillerRed-mediated ablation was carried out by immobilizing three to five L4 stage animals at a time using nanoparticles (3). Basically, three to five animals were picked into a small drop of 0.1-μm diameter polystyrene microspheres on a 10% (wt/wt) agarose pad and covered with a coverslip. Each animal was exposed for 3–5 min, focusing a green laser source on the cell body of targeted neurons. After illumination, animals were rescued with M9 buffer and cultivated at 15 °C or 25 °C for 1 d before being tested in the behavior assay. Neurons were reimaged after 1 d to verify destruction of the targeted neuron.

Caspase-mediated cell ablations were performed using a reconstituted caspase system (recCaspase) as previously described (4). Briefly, the two recCaspase components were driven in single cells using neuron-specific promoters (*gcy-8* for AFD, *glr-3* for RIA, and *ttx-3* for AIY). Transgenic animals expressing these constructs were generated using standard methods. To assess and quantify the efficiency of cell ablation with recCaspase, the recCaspase components were crossed into integrated reporter lines that allow fluorophore visualization in the neuron of interest [*wyIs111* for AFD and AIY (5) and *wyIs93* for RIA (6)], and loss of reporter fluorescence was scored using a compound microscope (model DM5000 G; Leica). The percentage of animals with surviving neurons was calculated by dividing the number of reporter fluorophore-positive animals by the total number of animals scored. Lines were scored multiple times for each condition (three times for AFD and RIA, twice for AIY) with 20–30 control and 20–30 array-carrying animals examined per scoring. For animals with the recCaspase coinjection marker, 67.8 ± 1.1% of *wyIs93* animals displayed loss of RIA, 80 ± 8.4% of *wyIs111* animals displayed loss of AFD, and 65.9 ± 2.3% *wyIs111* animals displayed loss of AIY. For all three ablation conditions (AFD, RIA, AIY), in the control group without the recCaspase coinjection marker, no neuronal ablation was observed, as expected. The same recCaspase transgenic arrays used in assessing ablation efficiency were used for behavioral testing. AIY-ablated animals were selected based on the absence of CFP in AIY.

Large-Format Behavioral Assay. A linear temperature gradient was generated on 22- × 22-cm agar plates by placing them on a black anodized aluminum platform (61 × 30 × 0.64 cm) bridged across the hot and cold aluminum reservoir blocks (10 × 30 × 3.8 cm). The cold reservoir temperature was maintained with a PID controller and H-bridge amplifier (Accuthermo), powered by a switching supply (Oven Industries) driving a thermoelectric cooler (TEC, Ferrotec) that pumped heat between the reservoir block and a liquid-cooled waterblock (Swiftech); the liquid was circulated with a pump and chiller unit (VWR). The hot reservoir was also controlled with PID feedback (Newport Electronics) that delivered current via a solid-state relay (Omega) to four resistive cartridge heaters (McMaster-Carr) embedded in the reservoir block. The temperature sensors (McMaster-Carr) used for both PID feedback loops were secured to the top plate near each reservoir block. Temperature at the agar gel surface was measured with a type T thermocouple probe (Physitemp) before and after each experiment to check for thermal drift; the same probe was used to systematically measure temperature in both horizontal dimensions on the surface. Temperature was constant in the direction perpendicular to the gradient.

The assay plate was illuminated by Super Bright LED bars. Movie S1 was captured using a 5-megapixel USB camera (Mightex) for 15 min at 2 fp using Mightex Camera Demo (V1.2.0). Trajectories were analyzed by adapting the MagatAnalyzer software package (7). To automatically flag reorientations and differentiate sharp turns and reversal turns, we considered both the posture of the animal and the movement of its center of mass. Rapid reorientations (sharp turns or reversal turns) were flagged when the heading change of the center of mass trajectory was >60° over 1 s. When the worm executes a sharp turn, the aspect ratio of the worm image decreases before the worm resumes forward movement in a new direction. When a worm executes a reversal, the aspect ratio remains high and the center of mass reverses its direction, backtracking along the original path. To quantify the aspect ratio, we took the ratio of the two eigenvalues of the covariance matrix of the pixel intensity recorded by the camera

(http://en.wikipedia.org/wiki/Image_moment). A larger ratio indicated that the worm was elongated and a smaller ratio indicated that the worm had assumed a more circular shape. Reversals were flagged as sudden reversals in trajectory within 20° of the reverse of the previous heading, maintaining an eigenvalue ratio of >1.8. Otherwise, reorientations were flagged as sharp turns.

High-Resolution Behavioral Analysis. A linear temperature gradient was generated on an agar surface using a smaller version (10 × 16 cm) of the apparatus that was used for high-throughput behavioral analysis. In this case, the entire temperature gradient assembly was placed on a Ludl Mac6000 Motorized Stage on an upright Nikon LV100 microscope. We used the Nikon Elements software package to manually control stage movements to keep the image of the worm in the center of the field of view and recorded the image of the worm at 4× magnification using an Andor Ixon Camera. The dorsal and ventral sides of each animal were manually labeled. Center-of-mass trajectories were calculated afterward using the recorded stage movements and images of the worm using custom scripts written in MATLAB (Mathworks).

Calcium Imaging. Worms were imaged on a custom-built temperature control stage using a spinning disk confocal microscope (Andor Technology), where a PID controller and H-bridge amplifier (Accuthermo) drove a thermoelectric cooler (TEC) (Newark) that pumped heat into and out of a thin copper plate (7.4 × 7.4 × 0.5 cm) with a liquid-cooled water block (Swiftech) acting as a thermal reservoir. A type-T thermocouple microprobe (Physitemp) was placed on the copper plate underneath a thin steel tab (7.4 × 2.5 × 0.013 cm). Transgenic worms expressing GCaMP6s (8) in AFD were placed on the steel tab directly above the temperature probe. Temperature was delivered by altering the PID controller's set point dynamically, using custom software written in LabVIEW (National Instruments). Because the temperature at the position of the worm could differ from the embedded thermocouple probe temperature, larval temperature was calibrated using a second probe taking the wworm's place while delivering the same temperature programs. Images from an EMCCD camera (Andor Technology) were recorded using either iQ (Andor Technology) or NIS Elements (Nikon Instruments) software.

1. Ramot D, MacInnis BL, Lee H-C, Goodman MB (2008) Thermotaxis is a robust mechanism for thermoregulation in Caenorhabditis elegans nematodes. *J Neurosci* 28(47):12546–12557.
2. Glauser DA, Johnson BE, Aldrich RW, Goodman MB (2011) Intragenic alternative splicing coordination is essential for Caenorhabditis elegans slo-1 gene function. *Proc Natl Acad Sci USA* 108(51):20790–20795.
3. Kim E, Sun L, Gabel CV, Fang-Yen C (2013) Long-term imaging of Caenorhabditis elegans using nanoparticle-mediated immobilization. *PLoS ONE* 8(1):e53419.
4. Chelur DS, Chalfie M (2007) Targeted cell killing by reconstituted caspases. *Proc Natl Acad Sci USA* 104(7):2283–2288.
5. Hellman AB, Shen K (2011) Sensory transduction channel subunits, tax-4 and tax-2, modify presynaptic molecular architecture in C. elegans. *PLoS ONE* 6(9): e24562.
6. Margeta MA, Wang GJ, Shen K (2009) Clathrin adaptor AP-1 complex excludes multiple postsynaptic receptors from axons in C. elegans. *Proc Natl Acad Sci USA* 106(5):1632–1637.
7. Gershow M, et al. (2012) Controlling airborne cues to study small animal navigation. *Nat Methods* 9(3):290–296.
8. Chen T-W, et al. (2013) Ultrasensitive fluorescent proteins for imaging neuronal activity. *Nature* 499(7458):295–300.

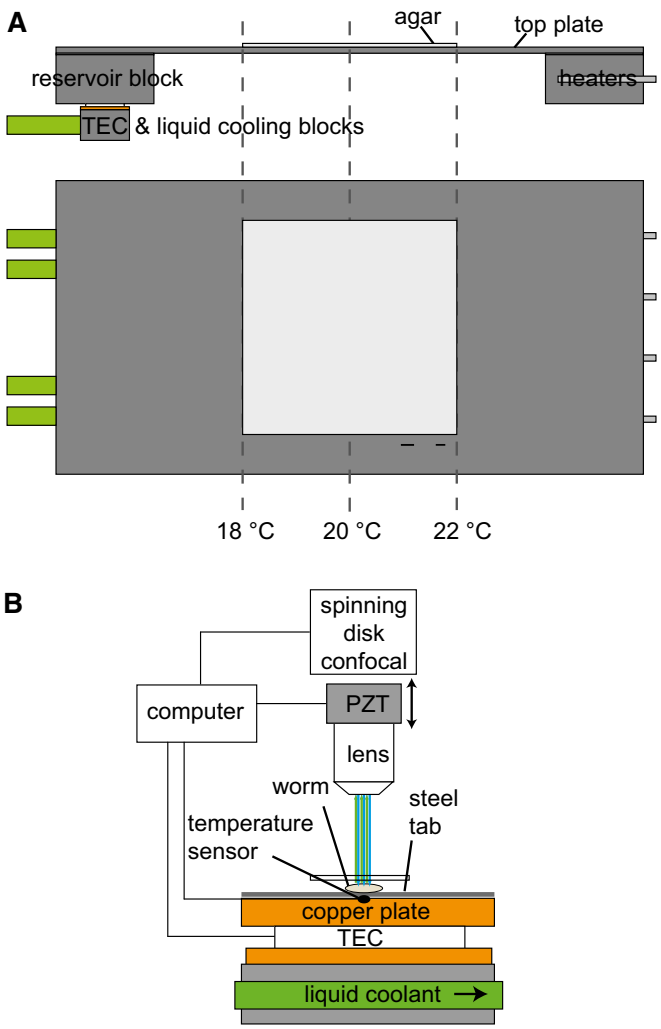

Fig. S1. Apparatus for behavioral and physiological analysis. (*A*) Schematic of spatial temperature gradient apparatus for tracking thermotaxis with stable cold and warm sides maintained to establish a linear gradient across the surface of a large agar gel. (*B*) Schematic of the microscope setup for calcium imaging. A custom temperature-controlled stage with objective focus feedback allows 3D confocal imaging during programmed temperature waveforms.

Movie S1. Overview of analysis. Playback of worms navigating a 22- × 22-cm plate under dark-field illumination, showing center-of-mass tracking of overall movement as well as high-resolution analysis of worm posture. Trajectories were segmented into alternating periods of forward movement, turns, and reversals on the basis of movement and posture as described in *Materials and Methods*. Playback is 15×.

Movie S1